ADVANCED MATERIALS

www.advmat.de

NIR Biosensing of Neurotransmitters in Stem Cell-Derived Neural Interface Using Advanced Core–Shell Upconversion Nanoparticles

*Hudifah Rabie, Yixiao Zhang, Nicholas Pasquale, Maureen J. Lagos, Philip E. Batson, and Ki-Bum Lee**

Nondestructive neurotransmitter detection and real-time monitoring of stem cell differentiation are both of great significance in the field of neurodegenerative disease and regenerative medicine. Although luminescent biosensing nanoprobes have been developed to address this need, they have intrinsic limitations such as autofluorescence, scattering, and phototoxicity. Upconversion nanoparticles (UCNPs) have gained increasing attention for various biomedical applications due to their high photostability, low autofluorescent background, and deep tissue penetration; however, UCNPs also suffer from low emission intensities due to undesirable energy migration pathways. To address the aforementioned issue, a single-crystal core–shell–shell "sandwich" structured UCNP is developed that is designed to minimize deleterious energy back-transfer to yield bright visible emissions using low power density excitations. These UCNPs show a remarkable enhancement of luminescent output relative to conventional β-NaYF4:Yb,Er codoped UCNPs and β-NaYF4:Yb,Er@NaYF4:Yb "active shell" alike. Moreover, this advanced core–shell–shell UCNP is subsequently used to develop a highly sensitive biosensor for the ultrasensitive detection of dopamine released from stem cell-derived dopaminergic-neurons. Given the challenges of in situ detection of neurotransmitters, the developed NIR-based biosensing of neurotransmitters in stem cell-derived neural interfaces present a unique tool for investigating single-cell mechanisms associated with dopamine, or other neurotransmitters, and their roles in neurological processes.

Stem cell research has provided promising solutions for treating progressing neurological disorders.[1] In particular, the generation of neurotransmitter-producing neurons, such as dopaminergic neurons (DA-neurons), from stem cells and their transplantation into damaged areas of the brain has shown encouraging therapeutic results for neurodegenerative diseases such as Parkinson's disease (PD).[2] In the case of PD, most patients lose more than 80% of their DA-neurons in the substantia nigra by the time motor symptoms, including bradykinesia, rigidity, and tremors, become present.[3,4] Therefore, the detection of neurotransmitters during stem cell differentiation and neuromodulation processes in the central nervous system (CNS) is of paramount importance for advancing stem cell-based therapeutics and studying neuropathological pathways involved in cellular processes. Such processes may include the biochemical conversion of L-DOPA to dopamine (DA), an essential neurotransmitter involved in modulating various neurophysiological processes.[5] Abnormal DA levels have been correlated with serious neurological disorders including PD,[6] schizophrenia,[7] and Huntington's disease.[8] Hence, developing a highly sensitive, selective, real-time, and noninvasive detection method for neurotransmitters at the single-cell level would be critical for gaining an insight into how neural interactions regulate brain functions, into developing better molecular diagnostics and therapeutics for neurological disorders, and into the evaluation of drug efficacy.

Conventional optical biosensors often possess a bright luminescent response to excitations; however, for bioimaging and optical biosensing, a high signal-to-noise ratio is much more important than luminescent output. This is due to the fact that there are major disadvantages regarding typical fluorescent probes that limit their use in biological systems including phenomena like autofluorescence, light scattering, and phototoxicity in response to commonly used UV–vis excitations. One class of phosphors with a particularly high signal-to-noise ratio includes lanthanide-doped upconversion nanoparticles (UCNPs).[9,10] UCNPs are a unique class

H. Rabie, Y. Zhang, Dr. N. Pasquale, Prof. K.-B. Lee
Department of Chemistry and Chemical Biology
Rutgers
The State University of New Jersey
Piscataway, NJ 08854, USA
E-mail: kblee@rutgers.edu

Dr. M. J. Lagos, Prof. P. E. Batson
Department of Physics
Rutgers
The State University of New Jersey
Piscataway, NJ 08854, USA

Prof. K.-B. Lee
Department of Life and Nanopharmaceutical Science
College of Pharmacy
Kyung Hee University
Seoul 02447, Republic of Korea

The ORCID identification number(s) for the author(s) of this article can be found under https://doi.org/10.1002/adma.201806991.

DOI: 10.1002/adma.201806991

of inorganic phosphors capable of absorbing near-infrared (NIR) light and converting it, through the sequential absorption of photons, to UV–vis emissions.[11] Coupled with their high photostability,[12] minimal background autofluorescence, and NIR excitation's ability to deeply penetrate biological tissues,[13] UCNPs have gained more and more attention in the fields of subcellular labeling,[14,15] in vivo bioimaging,[16,17] biosensing,[18–20] and optogenetics.[21–24] However, despite their great potential, even the most efficient upconversion material to date, codoped NaYF4:Yb,Ln (Ln = Lanthanide), remains with relatively poor upconversion efficiencies, especially in response to low-intensity laser excitation.[19,25–27] This is due to several factors such as (i) the low absorption cross-section of Yb^{3+}, which sensitizes the UCNPs to the absorption of 980 nm NIR light,[28] (ii) the parity forbidden nature of the 4f–4f transitions of the lanthanides,[29] (iii) and the use of relatively low concentrations of luminescent lanthanides to prevent quenching.[27] As such, UCNPs are typically excited with relatively high power density excitations, exceeding the safe threshold for many biological applications[16,30] due to the heating effect of 980 nm NIR excitation. Recent reports have demonstrated that high doping ratios, combined with interesting core@shell strategies can be used to mitigate this effect,[31–33] but further improvement would be beneifical to push the boundaries of the potential for the use of UCNPs in biomedical applications.

To overcome these limitations and further push the boundaries of biomedical technologies, it would be critical to develop UCNPs which can capitalize on low power density excitations and convert them to visible emissions. To this end, one of the most promising methods for increasing upconversion nanoparticle efficiency is the utilization of core–shell architectures. While previous core–shell methods addressed issues including surface defect-based quenching, Ln–Ln cross-relaxation, and dopant concentration tuning,[31] there is a clear need to investigate the Ln–Yb energy back-transfer mechanisms. Interestingly, it has been shown that red emissions from Er^{3+} doped $NaYF_4$ are resultant from a three-photon process involving energy back-transfer from the high lying $^4G/^2K$ manifold to the $^5F_{5/2}$ Yb^{3+} ground state. As such, energy back-transfer has a profound impact on the spectral profile, causing red emissions to occur at the expense of higher order green emissions, decreasing the overall luminescent intensity. Manipulating these energy migration dynamics can critically affect the ability of UCNPs to emit intense higher order visible emissions in response to low power density laser excitations, enhancing their potential in bioimaging, subcellular labeling, as well as biosensing.

Herein, we describe the innovative design and synthesis of a novel type of core-shell-shell "sandwich" structured UCNP [**β-$NaYF_4$: Yb^{3+}@ β-$NaYF_4$: Er^{3+} @ β-$NaYF_4$: Yb^{3+} (Yb@Er@Yb)**], which demonstrates relatively high luminescent output in response to low power density NIR excitations. Moreover, we demonstrate that these UCNPs can be combined with aptamers to be further utilized for detection of neurotransmitters from neural stem cell (NSC)-derived DA-neurons at the single-cell level in a highly sensitive, selective, real-time, and noninvasive manner. More specifically, the differentiation of human neural stem cells (hNSCs) into DA-neurons was confirmed using a nondestructive, real-time, and NIR-based detection method comprised of our developed UCNP-aptamer construct (**Figure 1**A).

In a typical experiment, we prepared our **Yb@Er@Yb** UCNPs in three steps, first by synthesizing a "sensitizing" nanoparticle core (SC) containing 20% Yb^{3+} as the only dopant following a reported method with modifications.[34] Second, we coated this nanoparticle core with a luminescent shell (LS) containing the emitting 2% Er^{3+} dopant, followed by a final "sensitizing" shell (SS) containing 20% Yb^{3+} only. This **Yb@Er@Yb** architecture serves to mitigate energy back-transfer from Er^{3+} ions' excited state to adjacent Yb^{3+} ions by spatially separating them into different layers to enhance desired two-photon emissions, while discouraging three-photon energy pathways. The rationale for this architecture is based on two phenomena that are exhibited in rare earth ion doped $NaYF_4$ upconversion nanoparticles. First, while rare earth ions' virtual energy states have relatively long lifetimes, they are still limited as they are excited energy states, and will deplete eventually to yield spontaneous emission. Second, resonance energy transfer (RET), the mechanism by which photon energy is transferred between the rare earth ions, is strongly affected by distance.[35] Furthermore, by isolating the sensitizers and activators in separate layers, the number of Yb^{3+} ions in close proximity to emitting Er^{3+} centers is decreased, therefore decreasing the probability of Er–Yb energy back-transfer without decreasing Yb^{3+} ion count (Figure 1B). Compared to traditional codoped structured **β-$NaYF_4$: Yb^{3+}/Er^{3+} (20%Yb/2% Er)**, or those coated with sensitizing shells **β-$NaYF_4$: Yb^{3+}/Er^{3+} @ β-$NaYF_4$: Yb^{3+} (20% Yb/2% Er@20% Yb)**, the **Yb@Er@Yb** "sandwich" structured UCNPs provide significantly more intense, two-photon process emissions due to the mitigation of Er–Yb energy back-transfer. As a proof of concept demonstration, this "sandwich" structured **Yb@Er@Yb** UCNP system was constructed into a highly sensitive NIR-based optical DA sensor with live cell DA detection capability (Figure 1A).

The general structure of the "sandwich" structured UCNP, as previously described, is composed of an activator (Er^{3+})-containing layer sandwiched between two sensitizing layers doped with Yb^{3+} (Figure 1B). This architecture allows for the inner and outer Yb^{3+} doped sensitizing layers to efficiently harvest 980 nm NIR excitation, funneling it towards the activator containing luminescent layer where it can promote the higher energy emissive states of the activator ions; however, considering the shell's thickness, emissions requiring three or more photons will be diminished due to the distance-dependent nature of RET.[35] Moreover, this specific arrangement of layers also minimizes the number of nearest neighbors between the activating lanthanides in the LS, sensitizing Yb^{3+} in the SC, and SS, therefore minimizing the probability of Er^{3+} to Yb^{3+} energy back-transfer (**Figure 2**A).

Following these general design considerations, we chose $NaYF_4$ as our host matrix due to its well-characterized nature, low lattice phonon energies, and relatively higher upconversion efficiencies when compared to other materials.[36] To construct our **Yb@Er@Yb** "sandwich" structure, as illustrated in (Figure 2A), we first synthesized a sensitizing core containing only 20% Yb^{3+} as a sensitizer (Figure 2B), which was then coated with a 10 nm thick activator-containing luminescent shell, doped with only the activator (2% Er^{3+}) (Figure 2B). The

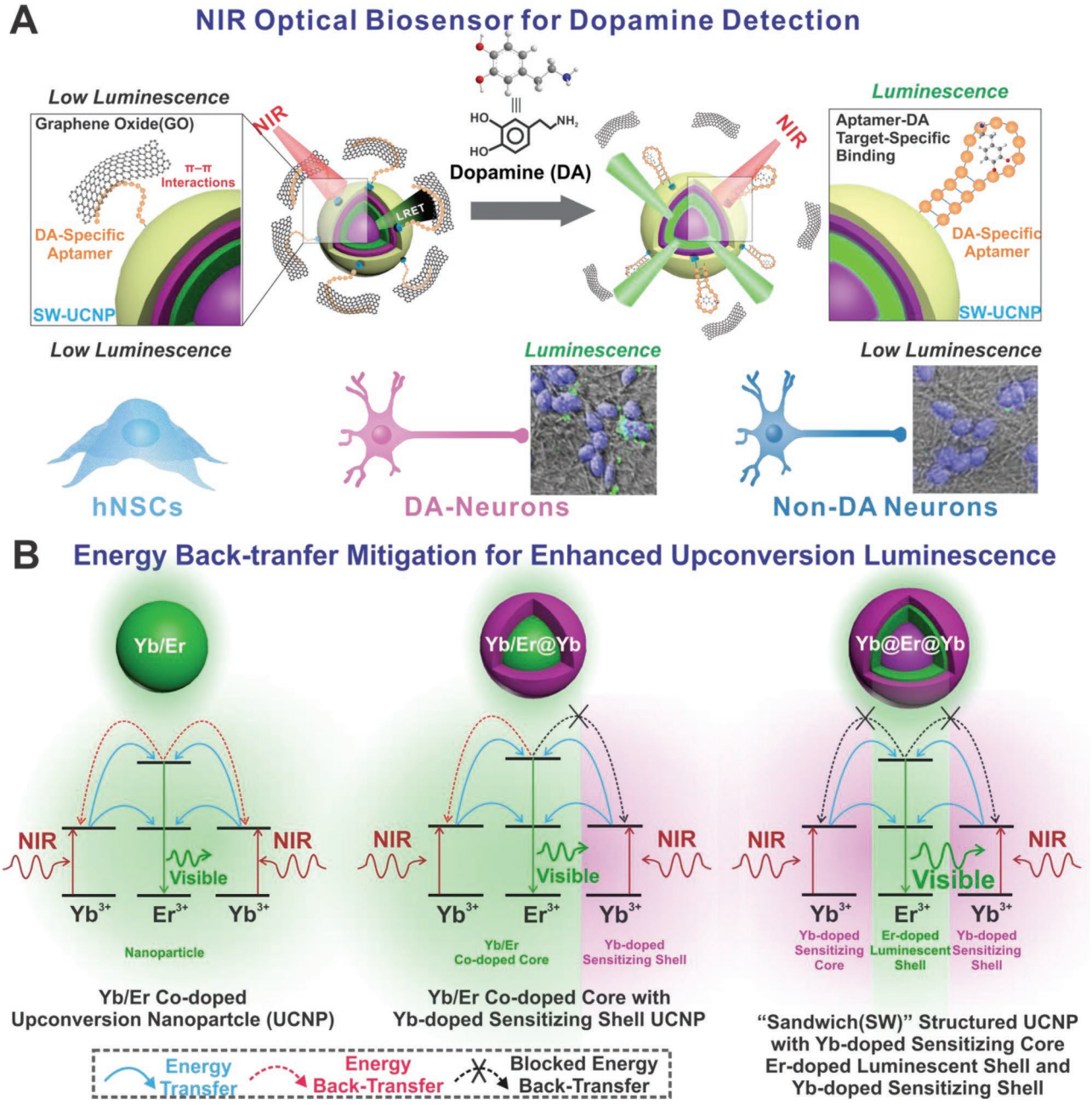

Figure 1. A) Schematic diagram of the constructed NIR-based dopamine sensor using the "sandwich" structured UCNP and its application in live cell dopamine sensing in non-DA-neurons and DA-neurons. Graphene-oxide based luminescence quenching is disrupted by the introduction of dopamine which interacts with aptamers to restore the upconversion luminescence from "sandwich" structured UCNPs. B) Schematic diagram comparing energy migration mechanisms among **Yb/Er** codoped UCNPs, **Yb/Er@Yb** "active-shell" UCNPs and the novel **Yb@Er@Yb** "sandwich" structured UCNPs. Left: codoped **Yb/Er** UCNPs, energy back-transfer (red arrows) from Er^{3+} to Yb^{3+} exists throughout the nanoparticle. Middle: "active shell" **Yb/Er@Yb** UCNPs, energy back-transfer (red arrows) from Er^{3+} to Yb^{3+} exists majorly in the Yb^{3+} and Er^{3+} codoped core. Right: the novel "sandwich" structured **Yb@Er@Yb** UCNPs, energy back-transfer is blocked (red arrows with cross) due to layered separation of Er^{3+} and Yb^{3+}. A more detailed schematic can be found in Figure S1 in the Supporting Information.

luminescent shell was specifically designed to be 10 nm thick, as this puts the innermost Ln ions of this layer within 5 nm of the Yb^{3+} doped layers, ensuring efficient energy migration to the luminescent Ln^{3+} centers[35] for up to two photons while mitigating further transfer. Finally, a 10 nm thick outer sensitizing shell (20% Yb^{3+}) was grown over the particle, sandwiching the luminescent shell between the Yb^{3+} containing sensitizing core and sensitizing shell, allowing for efficient energy migration to the luminescent lanthanide ions, and more intense upconversion emissions[35] (Figure 2B). High-resolution scanning transmission electron microscopy (HR-STEM) images show the monocrystalline nature of the as-synthesized **Yb@Er@Yb**

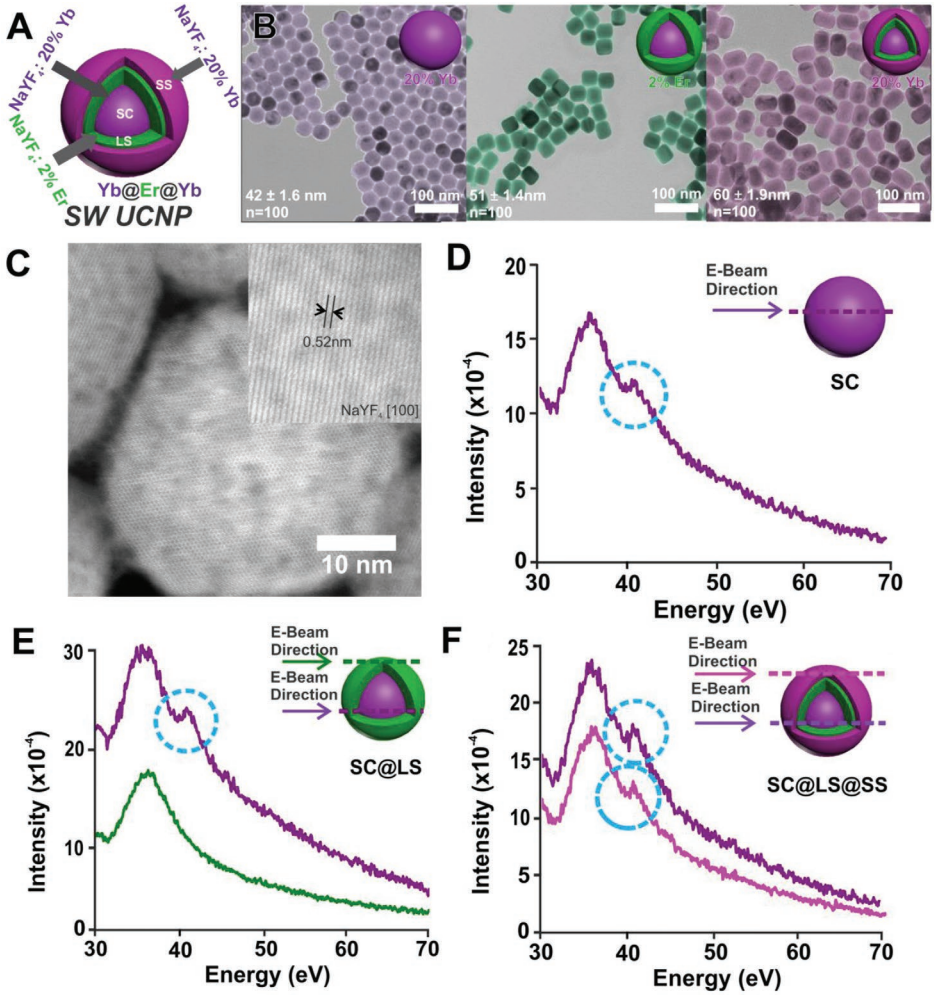

Figure 2. A) Schematic diagram of the designed **Yb@Er@Yb** "sandwich" structured UCNP. B) TEM images showing size and morphological evolution of the synthesized **Yb@Er@Yb** "sandwich" structured UCNP of 42 ± 1.6, 51 ± 1.4, 60 ± 1.9 nm respectively. C) High resolution STEM characterization of **Yb@Er@Yb** UCNPs. Inset shows the typical 0.52 nm lattice spacing of (100) crystallographic planes of β-$NaYF_4$. D) EELS spectrum of sensitizing core (SC). The shoulder peak highlighted by the blue circle at 40 eV is indicative of Yb^{3+} existence inside nanoparticle. E) EELS spectrum of luminescent shell coated sensitizing core (**SC@LS**). The characteristic peak of Yb^{3+} at 40 eV is present when the center of the UCNPs is exposed to the scanning electron probe (purple curve). On the contrary, when the scanning electron probe passes only edge (LS) of the nanoparticle, the 40 eV Yb^{3+} peak is absent, indicating the compositional separation of the two layers F) EELS spectrum of **Yb@Er@Yb** "sandwich" structured UCNPs. The Yb-specific peak at 40 eV is observed throughout the nanoparticle, since the electron probe always scans through a Yb^{3+} doped region after the SS layer growth.

"sandwich" UCNPs, which bear the characteristic lattice spacing of β-hexagonal $NaYF_4$ (Figure 2C).[37] To confirm the structural and compositional integrity of our core–shell architecture, we performed spatially-resolved step-by-step single particle electron energy loss spectroscopy (EELS) in to verify that Yb^{3+} is only detected in the SC and SS of the **Yb@Er@Yb** "sandwich" structure. In the EELS spectrum of the Yb^{3+} containing sensitizing core, the unique shoulder peak at 40 eV can be solely ascribed to the 5p to 5d transition of Yb^{3+}[38,39] (Figure 2D). Accordingly, this peak is only found when the EELS spectrum is taken in the SC and SS of our **Yb@Er@Yb** structured UCNPs (Figure 2D,F). The EELS data also points out the absence of the Yb^{3+} in the LS (Figure 2E), which is of significance for the upconversion luminescence study. This demonstrates our ability to synthesize the described sandwich structured UCNPs as corroborated by the TEM images in (Figure 2B).

Next, we studied the upconversion spectra of the as-synthesized **Yb@Er@Yb** UCNPs, which shows clear enhancement as can be seen in (**Figure 3**A). Comparing the upconversion luminescence of our **Yb@Er@Yb** UCNPs with typical **Yb/Er** codoped core UCNPs, a marked enhancement in green emissions of 80 times and total luminescent output of 63 times is shown (Figure 3B,C). Interestingly, our "sandwich" structured UCNP also compares favorably to "active shell" **Yb/Er@Yb** nanoparticles as well, showing a eight times green emission enhancement as well as six times total luminescent enhancement (Figure 3B,C). We speculate this is largely due to the mitigation of Er–Yb energy back-transfer, which occurs to a much greater extent in **Yb/Er** codoped core UCNP structures. This observation holds true when comparing **Yb/Er** codoped core UCNPs to "half sandwich" structured UCNPs (**Yb@Er**) of the same composition (20 mol% Yb^{3+} and 2 mol% Er^{3+}), where

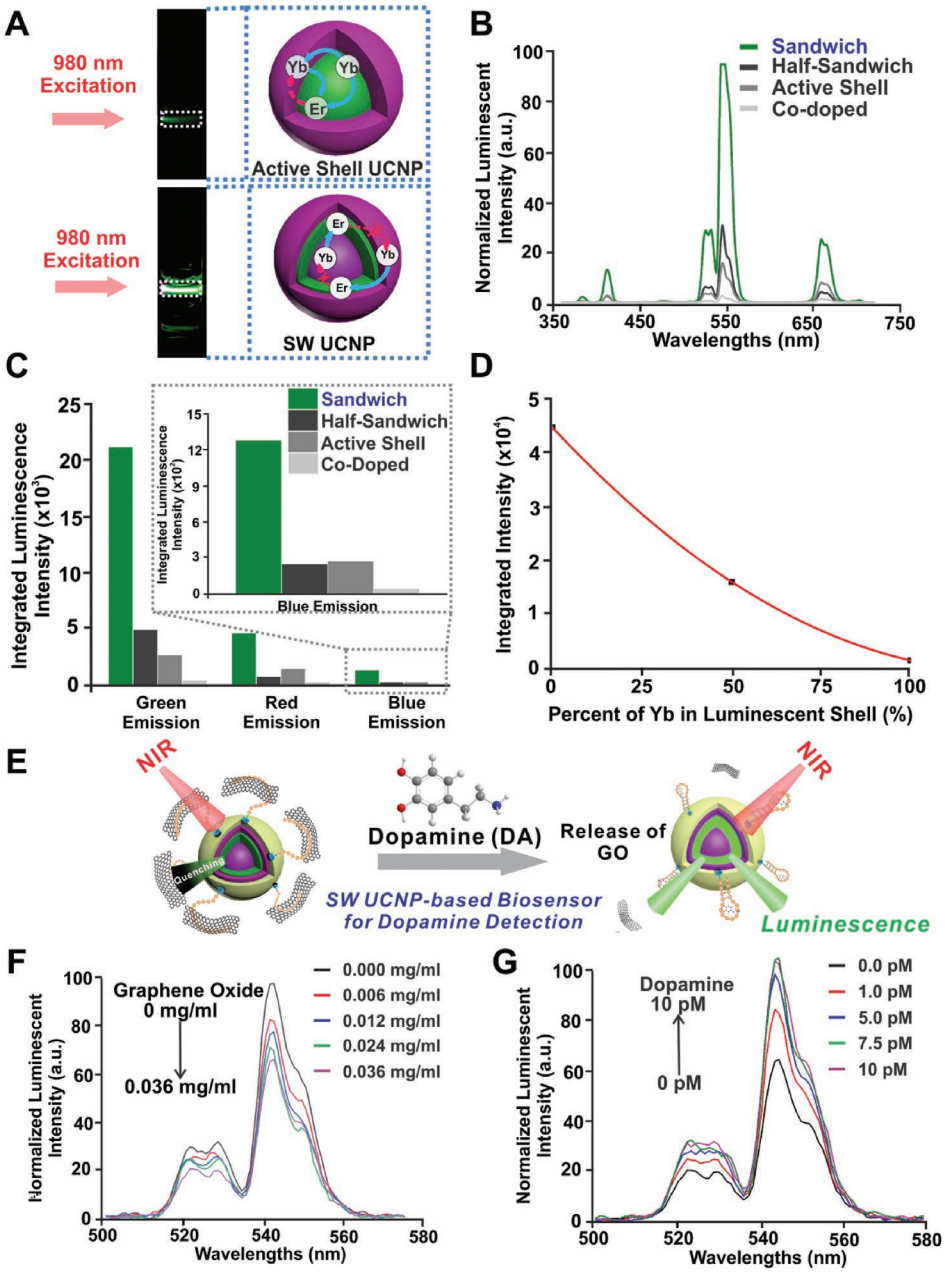

Figure 3. A) Photographs of **Yb/Er@Yb** (upper) and **Yb@Er@Yb** (lower) structured UCNPs in hexane solution (1 wt%) under same 980 nm laser excitation (25 W cm^{-2}). B) Upconversion luminescence profiles, demonstrating a large increase in luminescence from **Yb/Er** (codoped), **Yb/Er@Yb** (active shell), **Yb@Er** (half-sandwich), to **Yb@Er@Yb** (sandwich) UCNPs in response to the same 980 nm NIR excitation (25 W cm^{-2}). C) Bar chart shows the integrated luminescence intensity for the green, red, and blue emissions for the four types of UCNPs shown in inset (B). Note the large increase in the green emission and green to red ratios for "sandwich" structured **Yb@Er@Yb** UCNPs. D) Graph shows the decrease in integrated luminescence intensity when Yb^{3+} is included in the luminescent shell in **Yb@Er@Yb** "sandwich" structure UCNPs, allowing for energy back-transfer which leads to the decrease in luminescence intensity. E) Schematic diagram of the "sandwich" structured UCNP-based upconversion luminescence turn-on sensor. F) Upconversion luminescence quenching in response to cumulative graphene oxide coating. G) Upconversion luminescence increment in response to DA binding.

the only difference is the isolation of sensitizers and activators into separate shells, which mitigates the detrimental Er–Yb energy back-transfer, resulting in a 35% increase in green emissions (Figure 3C). Moreover, to further support that back-transfer mitigation is responsible for our enhancement, we have synthesized our sandwich structure with increasing Yb^{3+} mol% in the middle layer (LS) of the "sandwich" UCNPs, observing significant luminescence intensity decreases (Figure 3D).

The sandwich structured UCNPs' bright emissions in response to low power density excitations provides them with significant advantages in fields such as bioimaging, subcellular labeling, and biosensing. To demonstrate the utility of

the designed UCNPs, a simple luminescence resonant energy transfer (LRET)-based biosensor was constructed to sensitively detect DA at extremely low detection limits (pM) illustrated by the schematic in (Figure 3E). Dopamine is an important neurotransmitter which plays an important role in neuronal circuits involved in emotion, behavior, motor coordination, and addiction.[40] Moreover, the loss of DA-producing cells is a hallmark of PD, which currently affects up to ten million people worldwide.[41] To this end, it is essential to develop simple, robust, and sensitive biosensors capable of monitoring DA production and release from neurons.

To demonstrate NIR-based biosensing of neurotransmitters, a DA biosensor was constructed using our developed sandwich structured UCNPs. First, the UCNPs were coated with a silica shell to allow for facile surface chemistry and protection from luminescence quenching by water (Figure S6, Supporting Information). We then modified the silica shell with a customized aptamer specific for DA.[42,43] The presence of DA-specific aptamer on the surface of the UNCPs led to selective binding with DA molecules secreted during the NSC differentiation into DA-neurons. Lastly, to finish the assembly of our biosensor, we added graphene oxide (GO), prepared using a previously reported method,[44] (Figures S6 and S7, Supporting Information) at varying concentrations to the UCNP@SiO_2-aptamer complex. The DA aptamer interacts with the GO via pi–pi stacking between the GO and the nucleobases of the aptamer, quenching the UCNPs' fluorescence in a concentration-dependent manner[45] (Figure 3F). Upon the introduction and binding of DA with a 3 min equilibrium time, the aptamers take on their 3D shape, abrogating the pi–pi interactions with the GO, causing the release of GO and the commensurate recovery of luminescence[46] (Figure 3G).

Furthermore, due to the highly efficient upconversion process resulting from our "sandwich" structured UCNPs, we

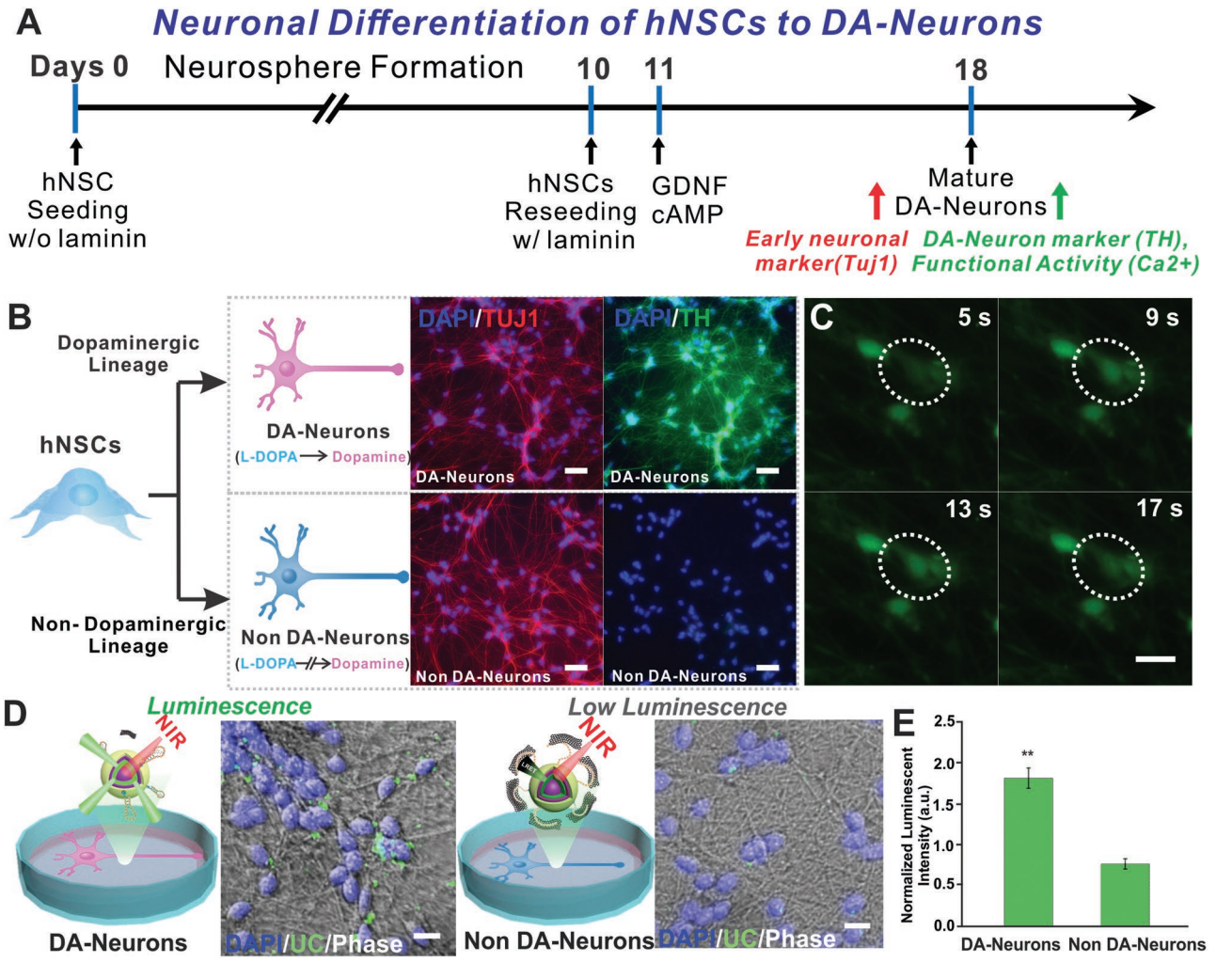

Figure 4. A) Schematic depicting the conversion of Neural Stem Cells (ReNcell VM) into DA-neurons. B) Immuno-fluorescence imaging characterizing DA-neurons and non-DA-neurons. Scale bar: 50 µm. (Blue: Nucleus (DAPI). Red: β tubulin (TUJ1). Green: Tyrosine Hydroxylase (TH).) C) Spontaneous calcium fluctuations determined by Fluo4 fluorescence for an active DA-neuron (white circle) during 17 s of imaging. Scale bar: 20 µm. D) Live cell upconversion luminescence imaging with DA and non-DA-neurons. Scale bar: 20 µm (Blue: Nucleus (DAPI). Green: Upconversion Luminescence (UC)) E) Live cell DA sensing quantitative comparison through microscope imaging signal. (Percent luminescence intensity increments are all normalized to live cell nucleus staining intensity as internal references). (Error bars represent mean ± s.d.; $n = 3$, ** $p < 0.01$, by one-way ANOVA with Tukey post-hoc test.)

were able to detect DA in a range of 1–10 pM with an $R^2 = 0.94$ (Figure S8, Supporting Information). This is three orders of magnitude more sensitive than previously demonstrated UCNP-LRET-based biosensors, which typically operate in the μM to nM range.[18,20,45,46] Critically, this has significant implications for the ability to monitor the in situ production of DA in the cytoplasm of neurons, as well as to study relevant diseases such as Alzheimer's and PD, where it is present in much lower concentrations.[47] For a proof-of-concept experiment, neural progenitor/stem cells (hNPSCs or hNSCs) with the ability to readily differentiate into neurons and glial cells were used[48,49] (**Figure 4**A). The hNSC-derived neurons can respond to extrinsic and intrinsic signals that further affect the neuronal fate in the CNS, which leads to subtype-specific neurons such as DA-neurons and GABAergic neurons. To confirm the dopaminergic and nondopaminergic differentiation of hNSCs respectively, cells were stained with tyrosine hydroxylase (TH), which is a representative marker of DA-neurons as shown in (Figure 4B). To further characterize the functionality of the DA-neurons, calcium imaging was conducted to monitor the changes in the intracellular calcium concentrations using a commercially available calcium indicator dye, Fluo4 (Figure 4C). Once the functionality of the DA-neurons was confirmed, showing appropriate biocompatibility with the synthesized DA sensors (Figure S9, Supporting Information), they were treated to detect the KCl triggered DA release by the two differentiated neuronal cell lines (Figure 4D). As expected, the biosensors in the DA-neurons showed brighter upconversion luminescence (Figure 4E). Additionally, the DA-neuron condition generated the highest luminescent increment when compared to various other conditions (Figure S11, Supporting Information). Interestingly, the luminescent increment of the nondopaminergic cell condition is very similar to that of the increment caused by the addition of the L-dopa alone (Figure S11, Supporting Information). Collectively, these results show that our NIR-based biosensor's luminescent recovery can not only sensitively detect DA, but can also be distinctly and directly correlated with L-dopa to DA conversion by normalizing for the difference in their response.

In summary, this work is a demonstration of a novel type of core–shell–shell "sandwich" structured, UCNP-based NIR sensing strategy focusing on DA detection during stem cell differentiation into subtype specific neurons at the single-cell level in a highly sensitive, selective, real-time, and noninvasive manner. This UCNP-based neurotransmitter sensing method can be used for detecting DA neuromodulation in vivo and be further extended to the development of novel diagnostics relevant to neurodegenerative diseases. These novel methods and applications also complement recent advances in UCNP-based brain imaging, nanomaterial-based biosensing of neurotransmitters, as well as conventional stem cell therapeutic strategies. While the ability to rationally design and synthesize a brighter Yb@Er@Yb "sandwich" structured UCNPs, using an energy back-transfer mitigation mechanism is critical for wide bioapplications of UCNPs, this uniquely designed UCNP specifically enables our system to produce bright visible emissions, 520 and 543 nm specifically, in response to relatively low power density excitations. The use of low power density 980 nm NIR excitation to produce bright emissions is critical in biological applications, as it mitigates the heating effect of 980 nm NIR excitations which is a long-standing challenge of using 980 nm NIR mediated upconversion nanomaterials. Furthermore, the enhanced visible emissions allowed us to demonstrate our architecture's functional utility in the form of a turn-on sensor, capable of detecting DA in low pM concentrations, which possesses an at least three-order of magnitude higher sensitivity comparing to similarly designed systems. Collectively, our NIR-based biosensing strategy to detect neurotransmitters in stem cell-derived neural interface using an advanced UCNP core–shell–shell architecture has significant potential for biomaterial science, neuroscience, and stem cell biology.

Supporting Information

Supporting Information is available from the Wiley Online Library or from the author.

Acknowledgements

H.R., Y.Z., and N.P. contributed equally to this work. The authors acknowledge partial financial support from the NIH R21 (1R21NS085569 and R21AR071101), NIH R01 (1R01DC016612-01 and 3R01DC016612-01S1), New Jersey Commission on Spinal Cord Research [CSCR17IRG010 and CSCR16ERG019], NSF [CHE-1429062 and CBET-1803517], and ACS New Directions Award (PRF# 55869-ND10). M.J.L. and P.E.B. acknowledge the financial support of US Department of Energy, Office of Science, Basic Energy Sciences under award number DE-SC0005132. The authors would also like to acknowledge Lisa M. Wiesholler and Professor Thomas Hirsch for help with upconversion luminescence lifetime characterization, and Dr. Letao Yang for synthesizing graphene oxide.

Conflict of Interest

The authors declare no conflict of interest.

Keywords

core–shell nanostructures, detection of dopamine, energy migration, neurotransmitters, NIR biosensors, stem cell differentiation, upconversion nanoparticles

Received: October 29, 2018
Revised: January 24, 2019
Published online:

[1] F. G. Teixeira, M. M. Carvalho, N. Sousa, A. J. Salgado, *Cell. Mol. Life Sci.* **2013**, *70*, 3871.
[2] R. A. Barker, M. Parmar, L. Studer, J. Takahashi, *Cell Stem Cell* **2017**, *21*, 569.
[3] H. C. Cheng, C. M. Ulane, R. E. Burke, *Ann. Neurol.* **2010**, *67*, 715.
[4] J. A. Obeso, M. Stamelou, C. G. Goetz, W. Poewe, A. E. Lang, D. Weintraub, D. Burn, G. M. Halliday, E. Bezard, S. Przedborski, S. Lehericy, D. J. Brooks, J. C. Rothwell, M. Hallett, M. R. DeLong, C. Marras, C. M. Tanner, G. W. Ross, J. W. Langston, C. Klein, V. Bonifati, J. Jankovic, A. M. Lozano, G. Deuschl, H. Bergman, E. Tolosa, M. Rodriguez-Violante, S. Fahn, R. B. Postuma, D. Berg, K. Marek, D. G. Standaert, D. J. Surmeier, C. W. Olanow,

J. H. Kordower, P. Calabresi, A. H. V. Schapira, A. J. Stoessl, *Mov. Disord.* **2017**, *32*, 1264.
[5] S. Navailles, M. Lagière, A. Contini, P. De Deurwaerdère, *ACS Chem. Neurosci.* **2013**, *4*, 680.
[6] K. M. Lohr, S. T. Masoud, A. Salahpour, G. W. Miller, *Eur. J. Neurosci.* **2017**, *45*, 20.
[7] T. D. Purves-Tyson, S. J. Owens, D. A. Rothmond, G. M. Halliday, K. L. Double, J. Stevens, T. McCrossin, C. Shannon Weickert, *Transl. Psychiatry* **2017**, *7*, e1003.
[8] C. Rangel-Barajas, G. V. Rebec, *J. Huntington's Dis.* **2016**, *5*, 303.
[9] M. Wang, G. Abbineni, A. Clevenger, C. Mao, S. Xu, *Nanomed.: Nanotechnol., Biol. Med.* **2011**, *7*, 710.
[10] Z. Li, Y. Zhang, X. Wu, L. Huang, D. Li, W. Fan, G. Han, *J. Am. Chem. Soc.* **2015**, *137*, 5304.
[11] F. Auzel, *Chem. Rev.* **2004**, *104*, 139.
[12] S. Wu, G. Han, D. J. Milliron, S. Aloni, V. Altoe, D. V. Talapin, B. E. Cohen, P. J. Schuck, *Proc. Natl. Acad. Sci. USA* **2009**, *106*, 10917.
[13] P. Ramasamy, P. Chandra, S. W. Rhee, J. Kim, *Nanoscale* **2013**, *5*, 8711.
[14] F. Wang, D. Banerjee, Y. Liu, X. Chen, X. Liu, *Analyst* **2010**, *135*, 1839.
[15] D. E. Achatz, R. Ali, O. S. Wolfbeis, *Top. Curr. Chem.* **2011**, *300*, 29.
[16] A. Nadort, V. K. Sreenivasan, Z. Song, E. A. Grebenik, A. V. Nechaev, V. A. Semchishen, V. Y. Panchenko, A. V. Zvyagin, *PLoS One* **2013**, *8*, e63292.
[17] G. Tian, Z. Gu, L. Zhou, W. Yin, X. Liu, L. Yan, S. Jin, W. Ren, G. Xing, S. Li, Y. Zhao, *Adv. Mater.* **2012**, *24*, 1226.
[18] S. Hao, G. Chen, C. Yang, *Theranostics* **2013**, *3*, 331.
[19] P. Huang, W. Zheng, S. Zhou, D. Tu, Z. Chen, H. Zhu, R. Li, E. Ma, M. Huang, X. Chen, *Angew. Chem., Int. Ed.* **2014**, *53*, 1252.
[20] L. Mattsson, K. D. Wegner, N. Hildebrandt, T. Soukka, *RSC Adv.* **2015**, *5*, 13270.
[21] S. Shah, J.-J. Liu, N. Pasquale, J. Lai, H. McGowan, Z. P. Pang, K.-B. Lee, *Nanoscale* **2015**, *7*, 16571.
[22] X. Wu, Y. Zhang, K. Takle, O. Bilsel, Z. Li, H. Lee, Z. Zhang, D. Li, W. Fan, C. Duan, E. M. Chan, C. Lois, Y. Xiang, G. Han, *ACS Nano* **2016**, *10*, 1060.
[23] L. He, Y. Zhang, G. Ma, P. Tan, Z. Li, S. Zang, X. Wu, J. Jing, S. Fang, L. Zhou, Y. Wang, Y. Huang, P. G. Hogan, G. Han, Y. Zhou, *eLife* **2015**, *4*, e10024.
[24] S. Chen, A. Z. Weitemier, X. Zeng, L. He, X. Wang, Y. Tao, A. J. Y. Huang, Y. Hashimotodani, M. Kano, H. Iwasaki, L. K. Parajuli, S. Okabe, D. B. L. Teh, A. H. All, I. Tsutsui-Kimura, K. F. Tanaka, X. Liu, T. J. McHugh, *Science* **2018**, *359*, 679.
[25] N. C. Dyck, F. C. J. M. van Veggel, G. P. Demopoulos, *ACS Appl. Mater. Interfaces* **2013**, *5*, 11661.
[26] S. Fischer, R. Martín-Rodríguez, B. Fröhlich, K. W. Krämer, A. Meijerink, J. C. Goldschmidt, *J. Lumin.* **2014**, *153*, 281.
[27] Q. Su, S. Han, X. Xie, H. Zhu, H. Chen, C. K. Chen, R. S. Liu, X. Chen, F. Wang, X. Liu, *J. Am. Chem. Soc.* **2012**, *134*, 20849.
[28] Y.-L. Wang, N. Mohammadi Estakhri, A. Johnson, H.-Y. Li, L.-X. Xu, Z. Zhang, A. Alù, Q.-Q. Wang, C.-K. Shih, *Sci. Rep.* **2015**, *5*, 10196.
[29] F. Vetrone, R. Naccache, V. Mahalingam, C. G. Morgan, J. A. Capobianco, *Adv. Funct. Mater.* **2009**, *19*, 2924.
[30] D. J. Gargas, E. M. Chan, A. D. Ostrowski, S. Aloni, M. V. Altoe, E. S. Barnard, B. Sanii, J. J. Urban, D. J. Milliron, B. E. Cohen, P. J. Schuck, *Nat. Nanotechnol.* **2014**, *9*, 300.
[31] B. Tian, A. Fernandez-Bravo, H. Najafiaghdam, N. A. Torquato, M. V. Altoe, A. Teitelboim, C. A. Tajon, Y. Tian, N. J. Borys, E. S. Barnard, M. Anwar, E. M. Chan, J. Schuch, B. E. Cohen, *Nat. Comm.* **2018**, *9*, 3082.
[32] H. Li, L. Xu, G. Chen, *Molecules* **2017**, *22*, 2113.
[33] Q. Liu, Y. Zhang, C. S. Peng, T. Yang, L.-M. Joubert, S. Chu, *Nat. Photonics* **2018**, *12*, 548.
[34] F. Wang, R. Deng, X. Liu, *Nat. Protoc.* **2014**, *9*, 1634.
[35] Y. Wang, K. Liu, X. Liu, K. Dohnalová, T. Gregorkiewicz, X. Kong, M. C. G. Aalders, W. J. Buma, H. Zhang, *J. Phys. Chem. Lett.* **2011**, *2*, 2083.
[36] D. Tu, Y. Liu, H. Zhu, R. Li, L. Liu, X. Chen, *Angew. Chem., Int. Ed.* **2013**, *52*, 1128.
[37] J. Lai, Y. Zhang, N. Pasquale, K. B. Lee, *Angew. Chem., Int. Ed.* **2014**, *53*, 14419.
[38] A. F. Orchard, G. Thornton, *J. Elec. Spec. Rel. Phen.* **1977**, *10*, 1.
[39] S.-i. Kimura, F. Arai, M. Ikezawa, *J. Phys. Soc. Jpn.* **2000**, *69*, 3451.
[40] M. J. Ferris, R. A. España, J. L. Locke, J. K. Konstantopoulos, J. H. Rose, R. Chen, S. R. Jones, *Proc. Natl. Acad. Sci. USA* **2014**, *111*, E2751.
[41] P. Hickey, M. Stacy, *Curr. Neurol. Neurosci. Rep.* **2012**, *12*, 376.
[42] R. Walsh, M. C. DeRosa, *Biochem. Biophys. Res. Commun.* **2009**, *388*, 732.
[43] E. Farjami, R. Campos, J. S. Nielsen, K. V. Gothelf, J. Kjems, E. E. Ferapontova, *Anal. Chem.* **2013**, *85*, 121.
[44] J.-H. Lee, H. K. Choi, L. Yang, S.-T. D. Chueng, J.-W. Choi, K.-B. Lee, *Adv. Mater.* **2018**, *30*, 1802762.
[45] C. Liu, Z. Wang, H. Jia, Z. Li, *Chem. Commun.* **2011**, *47*, 4661.
[46] Y. Wang, L. Bao, Z. Liu, D.-W. Pang, *Anal. Chem.* **2011**, *83*, 8130.
[47] T. M. Olefirowicz, A. G. Ewing, *J. Neurosci. Methods* **1990**, *34*, 11.
[48] Z. L. Chaudhry, B. Y. Ahmed, *Neurol. Res.* **2013**, *35*, 435.
[49] R. Donato, E. A. Miljan, S. J. Hines, S. Aouabdi, K. Pollock, S. Patel, F. A. Edwards, J. D. Sinden, *BMC Neurosci.* **2007**, *8*, 36.